Electron-ion recombination of Fe IV

Sultana N. Nahar, Manuel A. Bautista,* and Anil K. Pradhan
Department of Astronomy, The Ohio State University, Columbus, Ohio 43210
(Received 9 October 1997; revised manuscript received 4 February 1998)

Ab initio calculations are presented for total and partial recombination cross sections and rate coefficients for $e+\mathrm{Fe\ V}\rightarrow\mathrm{Fe\ IV}$, employing a unified treatment that incorporates both the radiative and dielectronic recombinations (RR and DR) in a self-consistent and accurate manner. The theoretical treatment is based on the close-coupling approximation using the *R*-matrix method. Recombination calculations for heavy atoms such as Fe IV, with $3d$ open-shell ground configuration, require an extensive eigenfunction expansion for the target ion, as well as a carefully optimized basis set of electron-ion bound configurations that represent short range correlation effects. The large-scale calculations are preceded by electron scattering and photoionization calculations using a 31-term eigenfunction expansion dominated by the configurations $3d^4$, $3d^3 4s$, and $3d^3 4p$ of Fe V. Photorecombination cross sections and DR collision strengths are thereby obtained, including individual photorecombination cross sections for a large number of bound states of Fe IV that couple to the ground state $3d^4\ ^5D$ of the target ion Fe V—all possible bound states up to $n=10$ (740 LS terms of Fe IV). The cross sections include autoionizing resonances, also up to the $n=10$ complex, accounting for the unified (RR + DR) contribution into the $n\leqslant 10$ (low-n) bound states of Fe IV. Recombination into the high-n states, $10\leqslant n\leqslant\infty$, is obtained through the DR collision strengths for the corresponding series of resonances in the electron-ion continua. The convergence of the close-coupling expansion, with respect to the target ion states and the (electron plus ion) correlation functions is discussed with reference to other highly complex atomic systems. Maxwellian average at a range of temperatures yields the total rate coefficient, as well as partial contributions directly to state-specific recombination rate coefficients. The new close-coupling rates differ considerably from those heretofore obtained from simpler approximations. We expect the present data to be of importance in the modeling of astrophysical and laboratory plasmas where iron is often a prominent constituent.
[S1050-2947(98)06912-1]

PACS number(s): 34.80.Kw, 32.80.Dz, 32.80.Fb

I. INTRODUCTION

The atomic physics of low ionization stages of heavy elements is characterized by complex electron-electron effects and associated phenomena such as autoionizing resonances that manifest themselves in important processes such as electron scattering, photoionization, and recombination. A theoretical treatment requires an *ab initio* consideration of these effects and phenomena since these processes are physically inter-related. Iron in low ionization stages, with $3d$ open shells and ground configurations $3d^n$, is an important example. Although astrophysical and laboratory spectra are rich in iron lines of different ionization stages, detailed and accurate calculations for the atomic parameters of these ions are difficult owing to the large number of highly coupled states and resonances. Prior to this work, no detailed calculations have been carried out for electron scattering or recombination of $e+\mathrm{Fe\ V}\rightarrow\mathrm{Fe\ IV}$. The computed atomic parameters are needed in the analysis of laboratory and astrophysical spectra, such as the determination of ionization fractions under photoionization equilibrium and spectral line intensities [1]. However, an equally important reason for these calculations is to study the nature and extent of the coupled states that are involved in scattering, photoionization, and recombination processes and determine the precision of related parameters for heavy atomic species in general.

As an application of the close-coupling approximation [2] to recombination processes, we have developed a unified treatment for electron-ion recombination that includes radiative recombination (RR) and dielectronic recombination (DR) in an accurate and *ab initio* manner [3–5]. The computational methods are extensions of those employed for large-scale calculations for photoionization and electron impact excitation under the Opacity Project (OP) [2] and the Iron Project (IP) [6]. In previous works, we have carried out such studies for the recombination of Fe I [7], Fe II [8], and Fe III [9], with extensive coupled channel calculations. Here we report on the study of $e+\mathrm{Fe\ V}\rightarrow\mathrm{Fe\ IV}$ recombination, and present both the total and the state-specific recombination rate coefficients.

The RR and the DR processes are always unified in nature, and in principle should be treated as such. In general the autoionizing resonances are inseparably embedded in the electron-ion continua; the contribution of the continuum or the resonances may not be treated individually. However, until our work on the unified treatment of recombination, it was usual practice to view RR as electron-ion recombination through the nonresonant background cross section alone, and DR as recombination through the autoionizing resonances alone; different approximations were employed for RR and DR. That such an approach is not physically correct is demonstrated by the presence of near-threshold autoionizing resonances that often dominate the photoionization (and

*Present address: Laboratory for High Energy Physics, Code 662, GSFC-NASA, Greenbelt, Maryland 20771.

hence the photorecombination) cross sections at low energies (temperatures). This low-energy DR has been considered, but separately and approximately, by Nussbaumer and Storey [10].

In the unified treatment, electron-ion recombination in the near-threshold region is dominated by recombination via the electron-ion continuum of the ground state, and by low-n resonances which couple the channels associated with the excited target levels included in the eigenfunction expansion for the (electron plus ion) system. Resonances are embedded in, and are an integral part of, the electron-ion continua, as manifest in the structure of the cross section for photoionization, the inverse process. The low-energy part of the present close-coupling calculations for photorecombination entails both the background and the resonances in the near-threshold region. At energies close to (but below) the series limits for the convergence of the Rydberg series of resonances, the recombination is dominated entirely by resonant recombination owing to the density of autoionizing resonances in those regions; the background contribution is negligibly small. In this region, below the series limits, the precise theory of DR developed by Bell and Seaton [11], using multichannel quantum defect theory and coupled channel (electron plus ion) wave functions, may be employed to compute the collision strengths for DR. Thus the close-coupling recombination cross sections may be obtained at both the low and high energies. Furthermore, the theortical treatment is self-consistent since the same eigenfunction expansion is used for both the photorecombination and the DR calculations.

The method has been extended to include relativistic effects in the Breit-Pauli approximation, using the Breit-Pauli R-matrix method, for highly charged ions [15–17]. However, electron-ion scattering calculations for the low ionization stages of iron, Fe II, III, and IV show the relativistic effects to be very small (e.g., [18,19]); these are therefore not considered in the present work. Although the close-coupling (CC) R-matrix calculations for $(e+\text{ion})$ recombination in the unified approach are very extensive, since they involve both the photoionization and electron-ion scattering calculations, the method has been successfully applied to obtain unified, total recombination rates for 33 atoms and ions so far.

While relativisitic effects are still small, but as the ion charge increases, the number of bound states that enter into the low-energy part of the $(e+\text{ion})$ recombination process increases rapidly with the ion charge. In addition, the accuracy of the close-coupling calculations in general depends on the completeness of the eigenfunction expansion which also involves bound channel $(e+\text{ion})$ correlation functions. We discuss the importance of these aspects of the calculations with respect to the unified method for electron-ion recombination.

II. THEORY

A. Close-coupling expansions

We employ the following notation. In the CC approximation the target (recombining ion) is represented by an N-electron system, and the recombined ion by an $(N+1)$-electron system. The total wave function expansion, $\Psi(E)$, of the $(N+1)$-electron system for any symmetry $SL\pi$ is represented in terms of the target wave functions as

TABLE I. Terms and energies, E_t (in Rydberg), of Fe V in the eigenfunction expansion of Fe IV.

Term	E_t	Term	E_t	Term	E_t
$3d^4(a^5D)$	0.0	$3d^34s(^3G)$	1.899	$3d^34p(^3G^o)$	2.404
$3d^4(^3P)$	0.227	$3d^34s(^3P)$	1.936	$3d^34p(^3F^o)$	2.429
$3d^4(^3H)$	0.227	$3d^34s(^3P)$	1.948	$3d^34p(z^5P^o)$	2.493
$3d^4(^3F)$	0.238	$3d^34s(^3D)$	1.965	$3d^34p(^3P^o)$	2.505
$3d^4(^3G)$	0.268	$3d^34s(^3H)$	1.970	$3d^34p(^3P^o)$	2.508
$3d^4(^3D)$	0.328	$3d^34s(^3F)$	2.123	$3d^34p(y^5D^o)$	2.517
$3d^4(^3P)$	0.561	$3d^34p(^5G^o)$	2.332	$3d^34p(^3H^o)$	2.522
$3d^4(^3F)$	0.561	$3d^34s(^3D)$	2.349	$3d^34p(^3G^o)$	2.540
$3d^34s(^5F)$	1.702	$3d^34p(z^5D^o)$	2.351	$3d^34p(^3F^o)$	2.550
$3d^34s(^3F)$	1.780	$3d^34p(z^5F^o)$	2.366		
$3d^34s(^5P)$	1.863	$3d^34p(^3D^o)$	2.368		

$$\Psi(E)=A\sum_i \chi_i\theta_i+\sum_j c_j\Phi_j, \tag{2.1}$$

where χ_i is the target wave function in a specific state $S_iL_i\pi_i$ and θ_i is the wave function for the $(N+1)$th electron in a channel labeled as $S_iL_i\pi_ik_i^2\ell_i(SL\pi)$, k_i^2 being its kinetic energy. Φ_j's are the correlation functions of the $(N+1)$-electron system that account for short range correlation and the orthogonality between the continuum and the bound orbitals.

As theoretical work on atomic systems of such complexity as the present case is rare, the full import of the short range correlations is largely unknown. Furthermore, this issue is made difficult to address owing to computational constraints since these bound channel functions require proportionally a much larger fraction of time than the first expansion over the target states. In most studies, the second basis set of Φ_j is chosen more or less empirically. For lighter atomic systems it is computationally feasible to include all $(e+\text{ion})$ bound states Φ_j that are consistent with the target states included in the first expansion of Eq. (1). However, for heavier atomic species the number of such bound channels is prohibitively large and a judicious choice needs to be made through trial and error based on the criteria of accurate energy levels for the computed $(e+\text{ion})$ bound states and the transition probabilities, as compared to available experimental data.

In the present CC calculations for Fe IV we employ an eigenfunction expansion, given in Table I, with the first expansion [Eq. (1), first summation of right-hand side] that is comprised of 31 states of Fe V [20], which includes terms from the ground $3d^4$, and the excited $3d^34s$, and $3d^34p$ configurations. The target wave functions were obtained using atomic structure code SUPERSTRUCTURE [21]. Observed energies for the target states (Table I) are used in the computations to ensure accurate positions for the resonances associated with the target states.

While the choice of the target state expansion for Fe IV is relatively straightforward, indeed somewhat smaller than similar expansions for Fe II and Fe III ([8] and [9], respectively), the set of correlation functions needed to achieve desired accuracy of radiative parameters is much more extensive. Table II gives the final list of the functions Φ_j [sec-

TABLE II. Correlation functions for Fe IV included in the CC expansion.

Even parity
$3p^63d^7, 3s^23p^43d^7, 3s3p^63d^6, 3p^63d^44s^24d,$ $3s3p^43d^74s, 3s3p^43d^74p, 3s3p^43d^74d, 3p^43d^74s^2, 3p^43d^74p^2,$ $3p^43d^64s4p^2, 3s^23p^63d^5, 3s^23p^63d^44s, 3p^63d^64s,$ $3p^63d^64d, 3p^63d^54s^2, 3p^63d^54p^2, 3p^63d^7, 3s^23p^53d^44s4p,$ $3p^63d^54s4d, 3s3p^63d^44s^2, 3s3p^63d^44p^2, 3s3p^63d^44s4d,$ $3p^63d^44s4p^2, 3s^23p^43d^54p^2, 3s^23p^43d^54s^2, 3s3p^63d^54s,$ $3s^23p^53d^44p4d, 3s3p^63d^6, 3s3p^63d^44s^2, 3s3p^63d^44p^2,$ $3s3p^63d^44s4d, 3s^23p^43d^7, 3s^23p^43d^64s,$ $3s^23p^43d^54s^2, 3s^23p^43d^54p^2, 3s^23p^43d^54s4d, 3s^23p^43d^44s4p^2,$ $3s^23p^63d^44d, 3s3p^63d^54d, 3s^23p^43d^64d, 3s3p^43d^44s^24p^2$
Odd parity
$3s3p^53d^7, 3p^53d^74s, 3p^53d^74p, 3p^53d^74d,$ $3s^23p^63d^44p, 3p^63d^64p, 3p^63d^54s4p, 3s3p^63d^44p4d,$ $3s^23p^53d^6, 3s^23p^53d^54s, 3s^23p^53d^54p, 3s^23p^53d^54d, 3p^63d^64s,$ $3s^23p^53d^44s4d, 3p^53d^64s4d, 3s^23p^53d^44s^2, 3s^23p^53d^44p^2,$ $3s3p^63d^44s4p, 3p^63d^44s^24p, 3s^23p^53d^44s4d, 3s3p^63d^44s4p$

ond summation on the right-hand side of Eq. (1)] employed in the present calculations for each parity. In principle one could include all electronic configurations, composed from the basis set of target orbitals, corresponding to all one-electron or two-electron or higher number of excitations from the orbitals of the ground configuration. Such a scheme, however, is neither computationally tractable nor necessary, since most of these correlate but weakly with the low-energy ($e+$ion) bound states. Therefore it is necessary to carry out several sets of calculations in order to make the final choice of the *total* CC expansion (target plus bound states). The complete CC expansions derived in this work should prove to be useful in future studies of atomic systems heavier than iron, in particular those along the same isoelectronic sequence as Fe IV.

B. Unified treatment of electron-ion recombination

General theoretical details of the calculations for recombination cross sections and rates using the unified treatment are described in Refs. [3–5,9]. In brief, we consider recombination into the infinite number of final recombined states of the ($e+$ion) system, divided into two groups: (A) recombination into low-n bound states ranging from the ground state to excited states with $n \leqslant n_{\max}$, and (B) recombination via high-lying resonances (DR) into the high-n bound states of the ($e+$ion) system with $n_{\max} \leqslant n \leqslant \infty$. Typical choice of $n_{\max}$ is 10. For group (A) states, we calculate the detailed photoionization cross sections (including autoionizing resonances) of the ground state and a large number of excited bound states up to all possible LS terms, $nSL\pi$, with n $\leqslant n_{\max}$. Photorecombination is related to photoionization by detailed balance (Milne relation) as

$$\sigma_{\mathrm{RC}} = \frac{g_i}{g_j} \frac{h^2\omega^2}{4\pi^2 m^2 c^2 v^2} \sigma_{\mathrm{PI}}. \tag{2.2}$$

where σ_{RC} is the photorecombination cross section, σ_{PI} is the photoionization cross section, ω is the photon frequency, v is the electron velocity, and g_i, g_j are the statistical weight factors of the recombining and recombined ions, respectively.

For the group (B) contribution, the DR collision strengths are calculated using the radiatively damped generalized scattering matrix, including the electron and photon channels, obtained from an application of the Bell and Seaton (BS) theory [11,4]. The complementarity between the electron-ion scattering collision strength for the dipole transition and the associated closed channel resonances contribution to DR is exact. The DR collision strength at threshold, as $n \to \infty$ from below, should be equal to the excitation collision strength due to electron impact at $E=0$. The BS theory of DR therefore provides a useful and accurate check on the DR calculations that can be independently verified by electron scattering calculations.

Another formulation of DR, suggested earlier by Hickman [12], entails the replacement of the core energies E_c by $E_c - iR/2$, where the complex part is the radiative decay rate. Hickman's approach represents a radiative optical potential based on intuitive arguments. Robicheaux [13] recently has shown that the Hickman formulation follows if certain approximations are not made in the BS theory. However, the practical differences between the two formulations are insignificant since they manifest themselves only for very large n, typically >1000 below an excited threshold. This has been discussed by Seaton [14], who points out that for a typical case, at all energies, the ratio of rates from the two theories differs from unity by less than one part in 10^5. Other uncertainties in the present calculations are larger (discussed later), primarily due to the choice of the eigenfunctions and numerical procedures associated with the R-matrix calculations.

III. COMPUTATIONS

Electron-ion recombination calculations involve both photoionization and electron scattering calculations in a self-consistent and complementary manner. The two sets of cal-

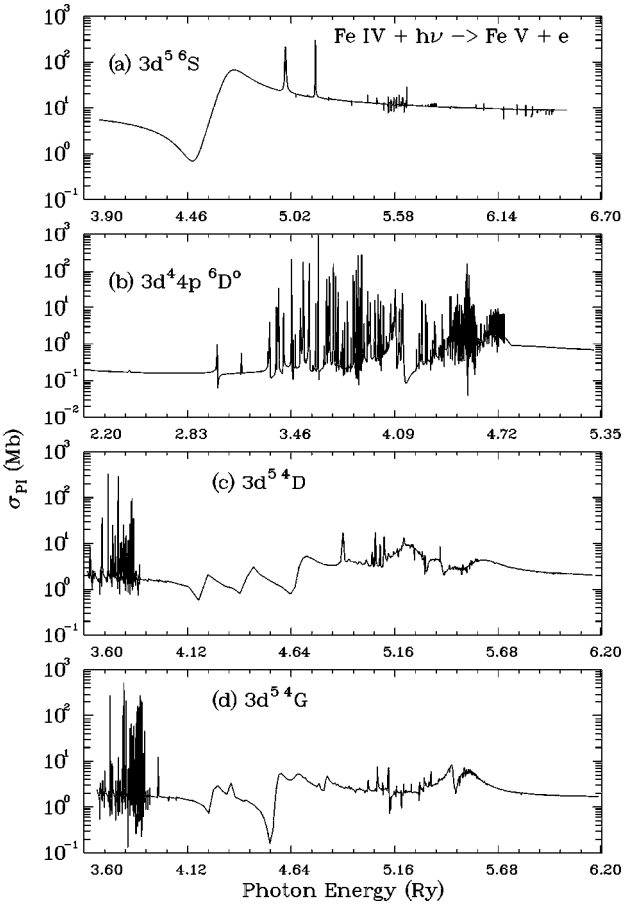

FIG. 1. Partial photoionization cross sections $\sigma_{\rm pi}(g)$ of Fe IV bound states: (a) the ground state $3d^5\,^6S$, (b) excited state $3d^4 4p\,^6D^o$, and the metastable states (c) $3d^5\,^4D$, (d) $3d^5\,^4G$; leaving the photoionized core ion Fe V in the ground state $3d^4\,^5D$.

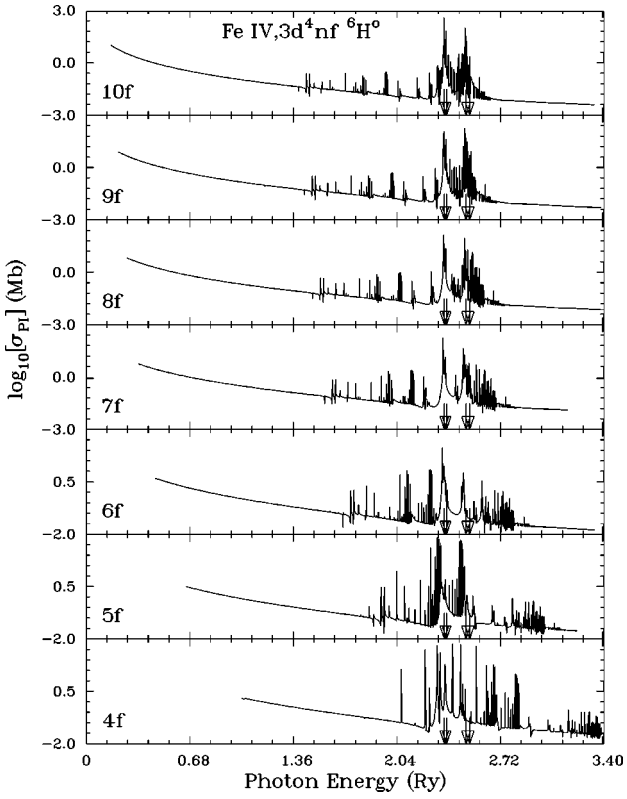

FIG. 2. Partial photoionization cross sections $\sigma_{\rm pi}(g)$ for the Rydberg series of Fe IV bound states, $3d^4nf\ ^6H^o(nf=4f-10f)$; positions of the PEC resonances are indicated by arrows.

culations, corresponding to low-energy or low-n and high-energy or high-n are described below.

A. Low-n states: Photorecombination

The group (A) ($e+$ion) bound state calculations for Fe IV yield 740 possible bound states $nSL\pi$ with $n\leqslant 10$. Of these 183 are sextets (spin multiplicity $2S+1=6$), and 557 quartets, coupled to the $3d^4(^5D)$ ground state of the target (core) ion Fe V. All of these contribute to the total recombination to Fe IV from the recombining Fe V in its ground state. The *partial* cross sections, $\sigma_{\rm PI}(g)$, of these states for photoionization into the ground state of Fe V are calculated as described in Ref. [20]. The computations are carried out employing the *R*-matrix codes from the Opacity Project [2] and the Iron Project [6], and a modified version of the program STGBF [5], to compute the bound-free partial cross sections. Recombination cross sections $\sigma_{\rm rc}$ are obtained from the $\sigma_{\rm pi}(g)$ through the Milne relation, and the recombination rate coefficients of individual bound states are obtained on convolving $\sigma_{\rm RC}(T)$ over the Maxwellian electron distribution at a given temperature *T*, using the code RECOMB [9]. The individual contributions from photorecombination cross sections of the 740 bound states of Fe IV are summed to obtain the group (A), or low-n, contribution to the total recombination rate coefficients α_R.

1. Photoionization cross sections

Some illustrative features of the photoionization cross sections are presented in Figs. 1 and 2, with relevance to their contributions to the total recombination rate coefficients. Fig. 1 presents $\sigma_{\rm pi}(g)$ of (a) ground $3d^5\,^6S$ state, (b) the excited state $3d^4 4p\,^6D^o$, and equivalent electron states (c) $3p^6 3d^5\,^4D$, (d) $3p^6 3d^5\,^4G$. These states, especially the equivalent states and the ground state, are among the dominant contributors to the total recombination rate coefficient α_R. Photoionization cross section of the ^6S ground state shows an extremely large resonance in the near-threshold region, which was identified as $3s^2 3p^5 3d^6(^6P^o)$, an equivalent electron configuration, that explains the broadness of the feature in contrast to the narrow Rydberg series of resonances $3s^2 3p^5 3d^5(^7P^o)nd(^6P^o)$. As described in Ref. [20], several sets of close-coupling calculations were required to determine the nature of this important feature in the low-energy region, Fig. 1(a), beyond which the background cross section remains high although no other comparable resonances are present. The equivalent electron states often have higher background cross sections, as also seen in Figs. 1(c) and 1(d), than the valence electron states, and thereby dominate photorecombination at low energies. In Fig. 1(b) we note that even though the $3d^4 4p\,^6D^o$ is a relatively highly excited state, recombination into this state becomes important at high temperatures via the extensive resonance structures at high energies.

2. Resonances due to photoexcitation of core or target states

Generally, the resonances at high energies may contribute significantly to recombination through the so called

TABLE III. Transition probabilities, A_{ji}, and collision strengths for EIE (with IPERT=0 and 1), and for DR, at the excited thresholds for dipole allowed transitions in Fe V.

Transition	A_{ji} (a.u.)	$\langle\Omega(\mathrm{DR})\rangle$	$\Omega(\mathrm{EIE})_0$	$\Omega(\mathrm{EIE})_1$
$a^5D^e \rightarrow z^5D^o$	2.16(−7)	5.79	5.63	5.63
$a^5D^e \rightarrow z^5F^o$	7.41(−8)	8.00	7.87	7.95
$a^5D^e \rightarrow z^5P^o$	1.89(−7)	3.28	3.19	3.19
$a^5D^e \rightarrow y^5D^o$	7.30(−9)	2.27	2.31	2.32

photoexcitation-of-core (PEC) resonances that appear as large features just below the target thresholds that are linked to the ground state by strong dipole transitions [22]. PEC may be considered as the inverse of the DR process contributing to low-n recombination. The PEC resonances are usually wider and may enhance the background cross section considerably, often by orders of magnitude. Recombination through the PEC's into the low-n states of the $(e+\mathrm{ion})$ system is a prime advantage of the unified CC method which accurately considers the energy profiles of these resonances. Since the PEC's are due to excitation of the core ion, they become more prominent in the photoionization of a Rydberg series of bound states with increasing n. Figure 2 presents the photoionization cross sections of the Rydberg series of states $3d^4nf\ ^6H^o$ of Fe IV, with nf from $4f$ to $10f$, where some of the PEC positions are indicated by arrows. In the target expansion of the 31 Fe V states (Table I), the target ground state $3d^4(a^5D)$ is linked through four dipole allowed transitions to z^5D^o, z^5F^o, z^5P^o, y^5D^o excited states, with corresponding PEC resonances (only two arrows can be seen distinctly in the figure since the energies of z^5D^o, z^5F^o, and of z^5P^o, y^5D^o are close together). Thus the PEC resonances can make important contributions to the recombination rate coefficients at higher temperatures.

B. High-n states: Dielectronic recombination

Recombination into the group (B) states, $n_{\max}<n\leqslant\infty$, of the $(e+\mathrm{ion})$ system is dominated by DR. It increases as ν^3, where ν is the effective quantum number relative to the threshold of convergence of the Rydberg series of resonances. Each series of autoionizing resonances is radiatively damped by the Einstein spontaneous decay rate A_r for the associated dipole transition between the ground state and an excited state of the target ion.

1. DR Collision strengths

Collision strengths for DR, $\Omega(\mathrm{DR})$, are calculated using the formulation described in [4] derived from the Bell and Seaton theory [11]. The $\Omega(\mathrm{DR})$ calculations are also carried out in the close-coupling approximation using the same 31-CC eigenfunction expansion used for the partial photoionization cross sections $\sigma_{\mathrm{pi}}(g)$. The radiative transition probabilities A_r for the dipole allowed transitions from the z^5D^o, z^5F^o, z^5P^o, and y^5D^o states to the ground state a^5D of Fe V are obtained from the oscillator strengths computed under the Iron Project [23] (given in Table III). The computations of $\Omega(\mathrm{DR})$ are carried out using the code STGFDR [4], which is an extension of the asymptotic region R-matrix code STGF [2].

$\Omega(\mathrm{DR})$ for the $(e+\mathrm{Fe\ V})$ system is calculated in two forms, detailed DR collision strengths with resonance profiles, and averaged over the resonances. Both sets of collision strengths are presented in Fig. 3; the dotted curve corresponds to the detailed form and the solid curve to the resonance averaged. Calculations start at $\nu=10.0$ below the target states. As seen from Fig. 3 (solid curve), DR is negligible for $\nu\leqslant 10$. $\Omega(\mathrm{DR})$ rises as the resonances become denser with increasing ν along the Rydberg series and converge on to the excited states (marked by arrows). The DR process peaks sharply near the thresholds of excitation. Physically, at

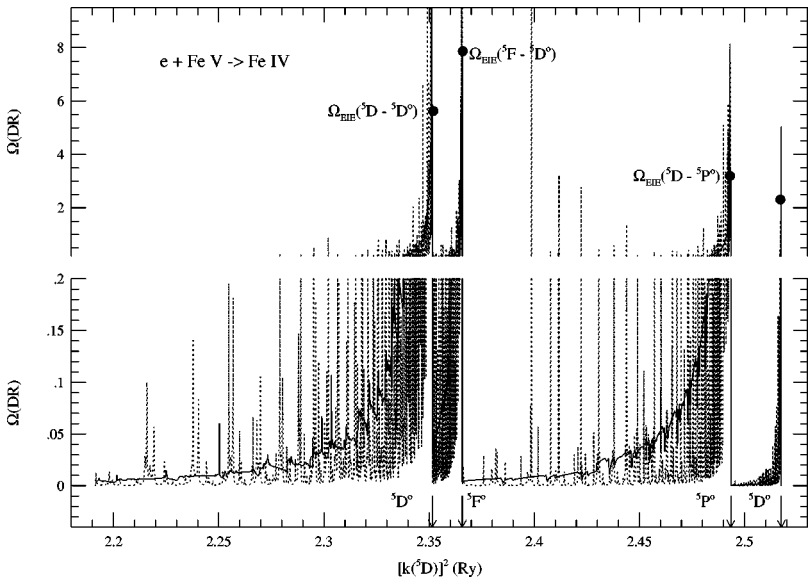

FIG. 3. DR collision strengths $\Omega(\mathrm{DR})$ for the dielectronic recombination of $e+\mathrm{Fe\ V}\rightarrow\mathrm{Fe\ IV}$: (i) with detailed resonances (dotted curves), and (ii) resonance averaged (solid curves). DR calculations start at effective quantum number $\nu=10$ of the Rydberg series of resonances belonging to the thresholds (pointed by the arrows) for dipole allowed transitions to the ground state $3d^5\ ^5D$ of Fe V. The filled circles are the excitation collision strength $\Omega(\mathrm{EIE})$ to which the $\langle\Omega(\mathrm{DR})\rangle$ converge.

energies below threshold the outer electron is loosely bound in high Rydberg resonances with increasingly small autoionization rates, $A_a \sim \nu^{-3}$, while the core damps radiatively at a constant rate A_r. Ω(DR) drops to zero at the thresholds when the trapped electron flux in the closed channel resonances is released through electron excitation of the core state. In principle then, Ω(DR) should equal Ω(EIE) (where EIE denotes electron impact excitation) at threshold. In practice, this provides a useful and stringent check on the DR calculations since Ω(EIE) may be computed independently (in some cases experimental measurements are available for dipole allowed transitions in electron impact excitation of ions). Some small features are seen in the resonance averaged curve due to interference effects with resonances belonging to thresholds higher than the threshold of convergence. In the computation of the total recombination rates we choose the resonance averaged Ω(DR), rather than the detailed, although the difference between the two sets is found to be less than 2%.

2. Collision strengths for DR and electron impact excitation

The filled circles in Fig. 3 are the collision strengths for electron impact excitation, Ω(EIE), for the corresponding dipole allowed transitions at threshold. These values are given in Table III. We carry out independent close-coupling (e + Fe V) scattering calculations for Ω(EIE), as a consistency check, with the same eigenfunction expansion as used in the computation of the DR collision strengths and the photoionization cross sections. It is also important to determine the effect of long range, higher-order multipole (nondipole) potentials neglected in multichannel quantum defect theory [4] as implemented in the Bell and Seaton theory [11]. This is ensured through a proper choice of the R-matrix boundary and the number of terms in the R-matrix basis set. Comparison between the excitation collision strengths, Ω(EIE), obtained getting a parameter in the code, IPERT=0 (exclusion of multipole potentials), and IPERT=1 (inclusion of multipole potentials), indicates the significance of the multipole potential contributions, as explained in [4]. The Ω(EIE) with IPERT = 0 and 1 for dipole allowed transitions in Fe V are presented in Table III; the two sets of values agree with each other to less than 1% for the four transitions, indicating that no significant error should result from the exclusion of nondipole potentials.

A further check is carried out for the conservation of flux between DR and EIE. As mentioned above, $\langle\Omega(\mathrm{DR})\rangle$ at each threshold should match Ω(EIE). From the values given in Table III, we find very good agreement between the two quantities at all of the thresholds of dipole transitions contributing to DR. Figure 3 also shows that the $\langle\Omega(\mathrm{DR})\rangle$ (solid curve) converges to Ω(EIE) (filled circles) at these thresholds to within $<10\%$. This is a crucial test for the calculations since $\langle\Omega(\mathrm{DR})\rangle$ and Ω(EIE) are computed with different formulations, the former employing the radiatively damped scattering matrix with (electron plus photon) channels defined in [11], and the latter from the usual undamped scattering matrix. Furthermore, the good agreement for a complex system such as Fe IV, with a large number of target states and coupled channels, lends confidence to the accuracy of the method and the computations.

TABLE IV. Total recombination rate coefficients, $\alpha_R(T)$, in units of cm^3 s^{-1}, for the recombination of e + Fe V→Fe IV. Numbers in brackets represent powers of 10.

$\log_{10}T$	α_R	$\log_{10}T$	α_R	$\log_{10}T$	α_R
1.0	5.57[-10]	3.1	2.93[-11]	5.2	5.85[-12]
1.1	4.88[-10]	3.2	2.53[-11]	5.3	6.11[-12]
1.2	4.28[-10]	3.3	2.18[-11]	5.4	6.03[-12]
1.3	3.74[-10]	3.4	1.88[-11]	5.5	5.64[-12]
1.4	3.27[-10]	3.5	1.64[-11]	5.6	5.01[-12]
1.5	2.86[-10]	3.6	1.45[-11]	5.7	4.31[-12]
1.6	2.49[-10]	3.7	1.28[-11]	5.8	3.58[-12]
1.7	2.17[-10]	3.8	1.15[-11]	5.9	2.90[-12]
1.8	1.89[-10]	3.9	1.03[-11]	6.0	2.32[-12]
1.9	1.65[-10]	4.0	9.14[-12]	6.1	1.81[-12]
2.0	1.43[-10]	4.1	8.06[-12]	6.2	1.41[-12]
2.1	1.24[-10]	4.2	7.03[-12]	6.3	1.08[-12]
2.2	1.08[-10]	4.3	6.06[-12]	6.4	8.32[-13]
2.3	9.38[-11]	4.4	5.19[-12]	6.5	6.37[-13]
2.4	8.13[-11]	4.5	4.48[-12]	6.6	4.51[-13]
2.5	7.06[-11]	4.6	3.93[-12]	6.7	3.40[-13]
2.6	6.11[-11]	4.7	3.63[-12]	6.8	2.56[-13]
2.7	5.29[-11]	4.8	3.62[-12]	6.9	1.90[-13]
2.8	4.57[-11]	4.9	3.95[-12]	7.0	1.42[-13]
2.9	3.95[-11]	5.0	4.56[-12]		
3.0	3.41[-11]	5.1	5.27[-12]		

In addition to the group (B) resonant contribution via DR, we also include the contribution from recombination through the nonresonant background for the high-n states through a ''top-up'' scheme as explained in Ref. [9]. Although this contribution is negligible at high energies and temperatures, it is considerable for low electron energies and very low temperatures when the resonances cannot be excited and recombination takes place only into the high-n states via the continuum. These background contributions may be calculated in the hydrogenic approximation with sufficient accuracy for all n [9].

IV. RESULTS AND DISCUSSIONS

Several aspects of the present calculations, in addition to the results obtained, are discussed below.

A. Total recombination rate coefficients

We obtain the unified total electron-ion recombination rate coefficients, $\alpha_R(T)$, and the individual state-specific recombination rate coefficients of a large number of bound states, for e + Fe V→Fe IV. The values of $\alpha_R(T)$ are presented in Table IV for a wide range of temperatures, $1.0 \leq \log_{10}T \leq 1.0$, at $\Delta\log_{10}T = 0.1$ to enable easy interpolation. The general features of $\alpha_R(T)$ are shown in Fig. 4: starting with high values at very low temperatures (solid curve) due to background continuum recombination to very high-n states, $\alpha_R(T)$ decreases to a minimum before rising to form a high-T bump at about $\log_{10}T = 5.3$ K, when the resonant recombination (DR) becomes dominant; thereafter α_R falls monotonically. In addition to the prominent high-T DR

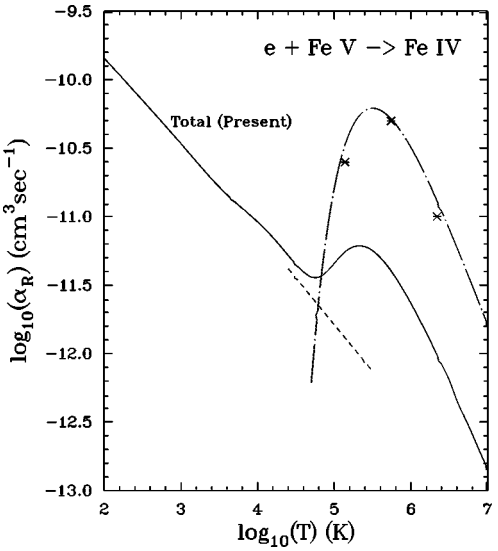

FIG. 4. Total recombination rate coefficients $\alpha_R(T)$ (solid curve) for Fe IV from the present work. Dashed curve corresponds to RR rates and the dot-dashed curve to DR rates, by Woods *et al.* [24]; the asterisks represent DR rates by Hahn [26].

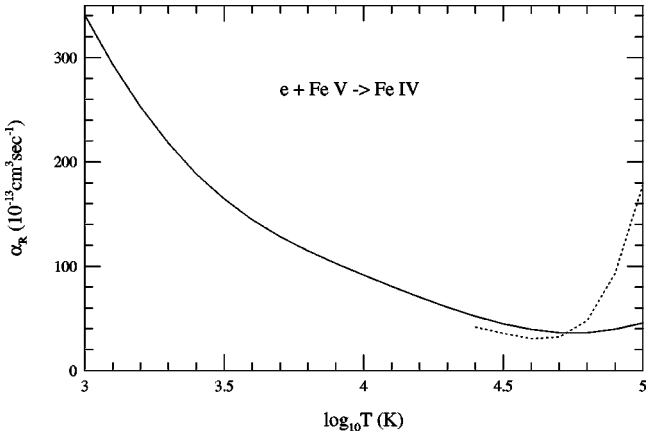

FIG. 5. $\alpha_R(T)$ on a linear scale shows differences with the earlier works not apparent on the logarithmic scale in Fig. 4. The dotted curve here is the *sum* of the (RR + DR) rates from Woods *et al.* [24]. It is noted that in general the log-log plots of the total e-ion recombination rates $\alpha_R(T)$ might obscure large differences, such as the low-T DR bump, that are clear on a linear scale (linear extrapolation on a log scale is incorrect and can be deceptive).

bump, the α_R also exhibits a slight low-T bump (seen for many other ions [5]) owing to low-energy autoionizing resonances in the cross sections leading to recombination into the low-n bound states [group (A)], i.e., the low-T DR first discussed in Ref. [10].

The present work reports the first calculations for electron-ion recombination of Fe IV considering resonance phenomena in detail. In previous works, Woods *et al.* [24] obtained the RR rate coefficients from photoionization cross sections in the central-field and the hydrogenic approximations that do not include resonances, and DR rate coefficients from the Burgess general formula [25]. They stated that the DR rates are uncertain because of an unreliable and incomplete set of oscillator strengths. Hahn [26] obtained the DR rates for recombination to Fe IV from an improved empirical formula, an extension of the Burgess general formula, but also commented on the uncertainty the atomic data employed.

Comparison of the present total recombination rate coefficient $\alpha_R(T)$ (solid curve) is made with the earlier works in Fig. 4, and large differences are found. The RR rates of Woods *et al.* [24] (dashed curve), valid over a small T range, underestimate the recombination rate significantly since their work does not include any resonance contributions at low energies. The sum of the Woods *et al.* (RR + DR) rates is shown in Fig. 5 (dotted curve). If extrapolated linearly this sum would differ with the present results at lower temperatures, including around $T=10^4$ K, near temperatures of maximum abundance of Fe IV in photoionization equilibrium [1]. These differences are partially due to the low-energy resonances that manifest themselves as a small hump in the low-T region ($T<10^4$ K) in Fig. 4. The DR rates by Woods *et al.* (dot-dashed curve in Fig. 4) considerably overestimate the recombination rate. In addition to possibly inaccurate oscillator strengths used in Ref. [24], there is an important effect of autoionization into excited states, not accounted for by the Burgess formula, that reduces the DR rate, as pointed out by Jacobs *et al.* [27]. Furthermore, the previous works do not take account of the strong couplings between all of the radiative and autoionization channels that are included in the present work in an *ab initio* manner.

B. Partial contributions to recombination rates

The individual state-specific recombination rates of the bound states are of importance in the determination of level populations and line intensities in nonlocal thermodynamic equilibrium (non-LTE) calculations of atomic spectra in laboratory and astrophysical plasmas. These rates for recombination into the first 20 states of Fe IV, from the sextet and quartet symmetries of group (A) bound states, are given in Table V. The states are listed according to their order of contributions to the total $\alpha_R(T)$ at $T=1000$, 10 000, 20 000, and 50 000 K. Both the order and the magnitude of contributions of these states vary with temperature because of resonance structures in photoionization cross sections. These rates represent only the direct photorecombination rate coefficients, and do not include possible high-n DR contribution (though that is not dominant until much higher temperatures ($T>10^5$ K). Therefore these rates do not represent the ''effective'' state-specific recombination rate coefficients since radiative cascades from higher states are not included.

C. Accuracy assessment and the close-coupling expansions

The accuracy of the present total recombination rate coefficients, $\alpha_R(T)$, may be estimated to be 10–30 % in the temperature range up to about 4.0×10^5 K, corresponding to the excitation temperature of the highest target state $^3F^o$ at energy 2.55 Ry explicitly included in the CC expansion (Table I). Therefore the present rates should be accurate at temperatures where Fe IV and Fe V are abundant under collisional or photoionization equilibrium in astrophysical or laboratory sources [1]. The uncertainties should be low since all states, and associated channels, are coupled together in the close-coupling treatment and the cross sections up to the

TABLE V. State-specific recombination rate coefficients (in units of $cm^3\ s^{-1}$) for $e + Fe\ V \rightarrow Fe\ IV$ at $T = 1000$, 10 000, 20 000, and 50 000 K. The first 20 states from the sextet and quartet symmetries are listed in order of their contributions; the percentage sum below refers to their combined contribution to the total $\alpha_R(T)$. Numbers in brackets represent powers of 10.

1000 K			10 000 K			20 000 K			50 000 K		
State		α_R	State		α_R	State		α_R	State		α_R
$3d^5$	$^6S^e$	8.56[-13]	$3d^5$	$^6S^e$	2.58[-13]	$3d^5$	$^6S^e$	1.83[-13]	$3d^5$	$^6S^e$	2.44[-13]
$3d^4\,^5D^e4s$	$^6D^e$	1.57[-13]	$3d^4\,^5D^e4s$	$^6D^e$	5.24[-14]	$3d^4\,^5D^e4s$	$^6D^e$	5.68[-14]	$3d^4\,^5D^e4s$	$^6D^e$	1.37[-13]
$3d^4\,^5D^e6g$	$^6H^e$	5.45[-14]	$3d^4\,^5D^e4d$	$^6G^e$	1.91[-14]	$3d^4\,^5D^e4d$	$^6G^e$	1.55[-14]	$3d^4\,^5D^e5s$	$^6D^e$	2.96[-14]
$3d^4\,^5D^e4d$	$^6G^e$	5.37[-14]	$3d^4\,^5D^e6g$	$^6H^e$	1.47[-14]	$3d^4\,^5D^e4d$	$^6F^e$	1.07[-14]	$3d^4\,^5D^e4d$	$^6G^e$	1.48[-14]
$3d^4\,^5D^e7g$	$^6H^e$	4.82[-14]	$3d^4\,^5D^e4d$	$^6F^e$	1.31[-14]	$3d^4\,^5D^e6g$	$^6H^e$	8.98[-15]	$3d^4\,^5D^e5d$	$^6G^e$	1.18[-14]
$3d^4\,^5D^e5g$	$^6H^e$	4.72[-14]	$3d^4\,^5D^e7g$	$^6H^e$	1.30[-14]	$3d^4\,^5D^e4d$	$^6D^e$	8.03[-15]	$3d^4\,^5D^e4d$	$^6F^e$	1.03[-14]
$3d^4\,^5D^e6g$	$^6G^e$	4.48[-14]	$3d^4\,^5D^e5g$	$^6H^e$	1.27[-14]	$3d^4\,^5D^e7g$	$^6H^e$	7.93[-15]	$3d^4\,^5D^e4d$	$^6D^e$	7.65[-15]
$3d^4\,^5D^e7g$	$^6G^e$	3.97[-14]	$3d^4\,^5D^e6g$	$^6G^e$	1.21[-14]	$3d^4\,^5D^e5g$	$^6H^e$	7.77[-15]	$3d^4\,^5D^e5d$	$^6F^e$	7.35[-15]
$3d^4\,^5D^e8g$	$^6H^e$	3.97[-14]	$3d^4\,^5D^e7g$	$^6G^e$	1.07[-14]	$3d^4\,^5D^e6g$	$^6G^e$	7.39[-15]	$3d^4\,^5D^e4d$	$^6P^e$	5.03[-15]
$3d^4\,^5D^e5g$	$^6G^e$	3.88[-14]	$3d^4\,^5D^e8g$	$^6H^e$	1.06[-14]	$3d^4\,^5D^e7g$	$^6G^e$	6.54[-15]	$3d^4\,^5D^e4d$	$^6S^e$	4.80[-15]
$3d^4\,^5D^e4d$	$^6F^e$	3.66[-14]	$3d^4\,^5D^e5g$	$^6G^e$	1.04[-14]	$3d^4\,^5D^e8g$	$^6H^e$	6.51[-15]	$3d^4\,^5D^e5d$	$^6P^e$	4.68[-15]
$3d^4\,^5D^e6g$	$^6F^e$	3.54[-14]	$3d^4\,^5D^e4d$	$^6D^e$	9.85[-15]	$3d^4\,^5D^e5g$	$^6G^e$	6.39[-15]	$3d^4\,^5D^e5d$	$^6D^e$	4.52[-15]
$3d^4\,^5D^e8g$	$^6G^e$	3.27[-14]	$3d^4\,^5D^e6g$	$^6F^e$	9.54[-15]	$3d^4\,^5D^e4d$	$^6S^e$	6.04[-15]	$3d^4\,^5D^e6g$	$^6H^e$	4.17[-15]
$3d^4\,^5D^e9g$	$^6H^e$	3.21[-14]	$3d^4\,^5D^e8g$	$^6G^e$	8.79[-15]	$3d^4\,^5D^e6g$	$^6F^e$	5.85[-15]	$3d^4\,^5D^e5g$	$^6H^e$	4.00[-15]
$3d^4\,^5D^e7g$	$^6F^e$	3.13[-14]	$3d^4\,^5D^e9g$	$^6H^e$	8.59[-15]	$3d^4\,^5D^e5s$	$^6D^e$	5.59[-15]	$3d^4\,^5D^e7g$	$^6H^e$	3.66[-15]
$3d^4\,^5D^e5g$	$^6F^e$	3.08[-14]	$3d^4\,^5D^e7g$	$^6F^e$	8.43[-15]	$3d^4\,^5D^e8g$	$^6G^e$	5.38[-15]	$3d^4\,^5D^e6g$	$^6G^e$	3.42[-15]
$3d^4\,^5D^e4d$	$^6D^e$	2.74[-14]	$3d^4\,^5D^e5g$	$^6F^e$	8.29[-15]	$3d^4\,^5D^e9g$	$^6H^e$	5.24[-15]	$3d^4\,^5D^e5g$	$^6G^e$	3.40[-15]
$3d^4\,^5D^e9g$	$^6G^e$	2.65[-14]	$3d^4\,^5D^e4d$	$^6S^e$	7.67[-15]	$3d^4\,^5D^e4d$	$^6P^e$	5.22[-15]	$3d^4\,^5D^e6s$	$^6D^e$	3.21[-15]
$3d^4\,^5D^e6g$	$^6D^e$	2.60[-14]	$3d^4\,^5D^e9g$	$^6G^e$	7.10[-15]	$3d^4\,^5D^e7g$	$^6F^e$	5.17[-15]	$3d^4\,^5D^e7g$	$^6G^e$	3.05[-15]
$3d^4\,^5D^e8g$	$^6F^e$	2.58[-14]	$3d^4\,^5D^e6g$	$^6D^e$	7.02[-15]	$3d^4\,^5D^e5g$	$^6F^e$	5.08[-15]	$3d^4\,^5D^e8g$	$^6H^e$	2.99[-15]
Sum=		1.69[-12]			5.02[-13]			3.69[-13]			5.10[-13]
Total=		3.41[-11]			9.14[-12]			6.06[-12]			3.63[-12]
%contribution=		5%			5%			6%			14%
$3d^5$	$^4G^e$	1.64[-12]	$3d^5$	$^4G^e$	1.41[-12]	$3d^5$	$^4G^e$	1.09[-12]	$3d^5$	$^4G^e$	5.83[-13]
$3d^5$	$^4D^e$	1.11[-12]	$3d^5$	$^4D^e$	7.24[-13]	$3d^5$	$^4D^e$	5.67[-13]	$3d^5$	$^4D^e$	2.99[-13]
$3d^5$	$^4F^e$	9.99[-13]	$3d^5$	$^4F^e$	6.43[-13]	$3d^5$	$^4F^e$	5.26[-13]	$3d^5$	$^4F^e$	2.91[-13]
$3d^5$	$^4P^e$	5.36[-13]	$3d^5$	$^4P^e$	2.61[-13]	$3d^5$	$^4P^e$	1.91[-13]	$3d^5$	$^4P^e$	1.09[-13]
$3d^4\,^3F^e5d$	$^4F^e$	1.45[-13]	$3d^4\,^3G^e4s$	$^4G^e$	6.28[-14]	$3d^4\,^3G^e4s$	$^4G^e$	6.86[-14]	$3d^4\,^3G^e4s$	$^4G^e$	7.77[-14]
$3d^4\,^3F^e5p$	$^4F^o$	1.45[-13]	$3d^4\,^5D^e4s$	$^4D^e$	3.40[-14]	$3d^4\,^5D^e4s$	$^4D^e$	2.64[-14]	$3d^4\,^5D^e4s$	$^4D^e$	2.64[-14]
$3d^4\,^5D^e4p$	$^4F^o$	1.05[-13]	$3d^4\,^5D^e4f$	$^4H^o$	2.95[-14]	$3d^4\,^5D^e4f$	$^4H^o$	1.92[-14]	$3d^4\,^3H^e4s$	$^4H^e$	2.17[-14]
$3d^4\,^5D^e4s$	$^4D^e$	1.03[-13]	$3d^4\,^5D^e5f$	$^4H^o$	2.52[-14]	$3d^4\,^5D^e5f$	$^4H^o$	1.65[-14]	$3d^4\,^5D^e4f$	$^4H^o$	1.15[-14]
$3d^4\,^5D^e4f$	$^4H^o$	1.02[-13]	$3d^4\,^5D^e4p$	$^4F^o$	2.36[-14]	$3d^4\,^3H^e4s$	$^4H^e$	1.64[-14]	$3d^4\,^5D^e4d$	$^4G^e$	1.06[-14]
$3d^4\,^3P^e5p$	$^4D^o$	9.74[-14]	$3d^4\,^5D^e4f$	$^4G^o$	2.14[-14]	$3d^4\,^3G^e4d$	$^4H^e$	1.64[-14]	$3d^4\,^5D^e4p$	$^4F^o$	1.04[-14]
$3d^4\,^3F^e4p$	$^4F^o$	9.13[-14]	$3d^4\,^3H^e4f$	$^4F^o$	1.95[-14]	$3d^4\,^5D^e4p$	$^4F^o$	1.52[-14]	$3d^4\,^5D^e4f$	$^4G^o$	9.20[-15]
$3d^4\,^5D^e5f$	$^4H^o$	8.76[-14]	$3d^4\,^5D^e5f$	$^4G^o$	1.91[-14]	$3d^4\,^3F^e4d$	$^4G^e$	1.39[-14]	$3d^4\,^5D^e5f$	$^4H^o$	8.68[-15]
$3d^4\,^3F^e6p$	$^4F^o$	8.46[-14]	$3d^4\,^5D^e4f$	$^4F^o$	1.73[-14]	$3d^4\,^5D^e4f$	$^4G^o$	1.38[-14]	$3d^4\,^5D^e4f$	$^4F^o$	7.95[-15]
$3d^4\,^3F^e5p$	$^4F^o$	7.92[-14]	$3d^4\,^3D^e4d$	$^4G^e$	1.70[-14]	$3d^4\,^3D^e4d$	$^4G^e$	1.35[-14]	$3d^4\,^3G^e4d$	$^4H^e$	7.69[-15]
$3d^4\,^3F^e7p$	$^4F^o$	7.51[-14]	$3d^4\,^3H^e5f$	$^4F^o$	1.68[-14]	$3d^4\,^5D^e4d$	$^4G^e$	1.29[-14]	$3d^4\,^5D^e4d$	$^4F^e$	6.77[-15]
$3d^4\,^5D^e4f$	$^4G^o$	7.45[-14]	$3d^4\,^5D^e6f$	$^4H^o$	1.66[-14]	$3d^4\,^5D^e5f$	$^4G^o$	1.24[-14]	$3d^4\,^3D^e4d$	$^4G^e$	6.72[-15]
$3d^4\,^5D^e4p$	$^4D^o$	7.12[-14]	$3d^4\,^3G^e4d$	$^4H^e$	1.66[-14]	$3d^4\,^3H^e4f$	$^4F^o$	1.17[-14]	$3d^4\,^3F^e4d$	$^4G^e$	6.62[-15]
$3d^4\,^5D^e5f$	$^4G^o$	6.58[-14]	$3d^4\,^5D^e4p$	$^4D^o$	1.65[-14]	$3d^4\,^5D^e4f$	$^4F^o$	1.13[-14]	$3d^4\,^5D^e5f$	$^4G^o$	6.55[-15]
$3d^4\,^5D^e5p$	$^4F^o$	6.09[-14]	$3d^4\,^5D^e4d$	$^4G^e$	1.62[-14]	$3d^4\,^5D^e6f$	$^4H^o$	1.09[-14]	$3d^4\,^5D^e4p$	$^4D^o$	6.20[-15]
$3d^4\,^5D^e4f$	$^4F^o$	6.03[-14]	$3d^4\,^5D^e5f$	$^4F^o$	1.53[-14]	$3d^4\,^5D^e4p$	$^4D^o$	1.03[-14]	$3d^4\,^5D^e4d$	$^4D^e$	6.14[-15]
Sum=		5.73[-12]			3.41[-12]			2.67[-12]			1.51[-12]
Total=		3.41[-11]			9.14[-12]			6.06[-12]			3.63[-12]
%contribution=		17%			37%			44%			42%

highest target threshold are accurately calculated including, in particular, the autoionizing resonances which are delineated in detail at a fine mesh of several thousand energies. The accuracy estimate is also based on an analysis of the agreement between the calculated and the observed energies of the bound states of Fe IV [20], generally a few percent, and the overall agreement between the length and the velocity oscillator strengths for a large number (a total of 34 635)

of transitions in Fe IV. The accuracy of the bound-bound transition probabilities is a direct indicator of the accuracy of the bound-free photoionization cross sections computed within the same formalism and with the same eigenfunction expansion. The Fe V target energies, as shown in Table I, also agree with observations to a few percent overall. Accurate target eigenfunctions are important in the CC approximation, and can be employed in *R*-matrix calculations for photoionization/photorecombination, electron-ion scattering, and DR cross sections.

A possible source of uncertainty in the recombination rates for $T>10^5$ K, is the truncation of the CC expansion beyond the $3d^4 4p(^3F^o)$ state of Fe V at 2.55 Ry. We do not expect a large contribution due to these highly excited target states in the eigenfunction expansion for reasons discussed below. The PEC resonances associated with increasingly higher target thresholds get weaker due to the enhanced probability of autoionization into additionally available states, resulting in a decrease in the DR collision strengths. The exponential decay of the Maxwellian in the rate integral also ensures that the contribution from highly excited states gets smaller with increasing energy (Ref. [8]); $\exp(-\epsilon/kT) = 0.02$ at $T=10^5$ K and $\epsilon=2.5$ Ry. We may estimate the position of the neglected $n=5$ Fe V states, linked to the ground state $3d^4(^5D)$ via dipole transitions, using the quantum defect of the $3d^3 4p(^5D^o)$ state at 2.52 Ry (Table I). Quantum defect extrapolation yields the $3d^3 5p(^5D^o)$ to lie at approximately 4.05 Ry, corresponding to an excitation temperature $T\approx 638\,000$ K. Therefore it may be concluded that at $T\approx 5\times 10^5$ K or less the present rates should be accurate to about 10–30% and the truncated states in the CC expansion contribute negligibly; however, the uncertainties are higher at higher temperatures. While not so in the present case, according to the arguments given above, the incompleteness of the CC eigenfunction expansion is expected to become more severe with increasing ion charge when the number of $(e+\text{ion})$ bound states, with the excited n complexes as parent core states, increases. This is discussed by Seaton *et al.* [28] with reference to iron ions with open $n=2$ and 3 shells ($3s$ and $3p$ open subshells in ionization states Fe IX and higher). Therefore, in addition to the resonant contributions at high energies due to DR via the high-n resonance complexes, we need to consider photorecombination via a large number of group (A) states that would also entail the same resonance complexes.

D. Radiation damping of autoionizing resonances

Narrow autoionizing resonances may be damped radiatively if their autoionization rates A_a are smaller than or comparable to the radiative decay rates A_r. This may occur for sufficiently high ion charge z, or the quantum numbers n or l. In the present work we do not consider possible radiation damping of low-n ($n<10$) autoionizing resonances in this work, since previous works have shown it to be of significance only for H-like and He-like ions [16,17]. For all low-z systems, such as Fe IV, radiation damping should be negligible. It should be noted, however, that the DR treatment included in the present work accounts for radiation damping of all resonances with $10\leqslant\nu\leqslant\infty$, and as shown in Fig. 3 the Ω(DR) is negligible for $\nu\leqslant 10$. As the autoionization rates decrease to zero as $n\rightarrow\infty$, and the radiative width increases relative to the separation between successive resonances in a Rydberg series, the resonance structures are broadened, smeared, and then wiped out (in that order). The BS theory predicts this behavior that is borne out by calculations [27]. In the limit of very high n there may be certain differences between the BS formulation and that of Robicheaux [13], which although not of practical importance as mentioned earlier, might lead to some differences at the threshold. However, these would require special sensitivity studies not necessarily related to the calculation of total recombination rates.

V. CONCLUSION

The main conclusions of the present work are as follows.

(i) The present study for Fe IV differs from those carried out earlier for less ionized species of iron in that it was found necessary to include a much larger set of bound channel configurations (Table II). The complete eigenfunction expansion given herein is likely to be useful in further studies or close-coupling calculations for electron scattering, photoionization, and recombination of heavier elements, particularly those within the iron group: cobalt, nickel, copper, and zinc, in ionization stages isoelectronic with Fe IV.

(ii) The target states to be included in close-coupling calculations for DR for more highly ionized species would need to include higher-n complexes that might be excited by the high-energy electrons in high-temperature plasmas. Target levels with $n=5$ or higher should be considered (e.g., configurations of the type $3d^n 5l$) in the calculation of DR collision strengths for heavier elements that are more ionized than Fe IV.

(iii) Total and state-specific recombination rate coefficients are presented for the recombined ion Fe IV obtained using the *R*-matrix method and a unified treatment within the CC formulation. The results of this first detailed study differ considerably from currently available values from approximations neglecting resonance phenomena, and DR rates from the Burgess formula. These recombination rates, along with the photoionization cross sections obtained in the CC approximation [20], provide self-consistent atomic data sets for accurate calculations of ionization balance under photoionization equilibrium [29,1]. This work forms part of a systematic computation of photoionization and recombination cross sections and rates for elements of astrophysical and technological importance, as exemplified by the recent work on all carbon and nitrogen ions [29], oxygen ions [30], the carbon isoelectronic sequence of ions [31], and the iron ions Fe I–III [7–9].

This study could be of potential interest in future work on heavy atoms within and beyond the iron group. Much more work is needed in understanding the nature of wave function expansions and their selective optimization for large close-coupling calculations as they are extended to higher rows of the Periodic Table [32].

ACKNOWLEDGMENTS

The work was supported by a NSF grant for the Iron Project (Grant No. PHY-9421898), and by NASA Grant No. NAGW-3315 and NAS-32643.

[1] M. A. Bautista and A. K. Pradhan, Astrophys. J **492**, 650 (1998).
[2] M. J. Seaton, J. Phys. B **20**, 6363 (1987); K. A. Berrington, P. G. Burke, K. Butler, M. J. Seaton, P. J. Storey, K. T. Taylor, and Yu. Yan, *ibid.* **20**, 6379 (1987) (OP).
[3] S. N. Nahar and A. K. Pradhan, Phys. Rev. Lett. **68**, 1488 (1992).
[4] S. N. Nahar and A. K. Pradhan, Phys. Rev. A **49**, 1816 (1994).
[5] S. N. Nahar and A. K. Pradhan, Astrophys. J. **447**, 966 (1995).
[6] D. G. Hummer, K. A. Berrington, W. Eissner, A. K. Pradhan, H. E. Saraph, and J. A. Tully, Astron. Astrophys. **279**, 298 (1993). (IP).
[7] S. N. Nahar, M. A. Bautista, and A. K. Pradhan, Astrophys. J. **479**, 497 (1997).
[8] S. N. Nahar, Phys. Rev. A **55**, 1980 (1997).
[9] S. N. Nahar, Phys. Rev. A **53**, 2417 (1996).
[10] H. Nussbaumer and P. J. Storey, Astron. Astrophys., Suppl. Ser. **64**, 545 (1986).
[11] R. H. Bell and M. J. Seaton, J. Phys. B **18**, 1589 (1985).
[12] A. P. Hickman, J. Phys. B **17**, L101 (1984).
[13] F. Robicheaux, J. Phys. B **31**, L109 (1998).
[14] M. J. Seaton, J. Phys. B (to be published).
[15] H. L. Zhang and A. K. Pradhan, Phys. Rev. Lett. **78**, 195 (1997).
[16] A. K. Pradhan and H. L. Zhang, J. Phys. B **30**, L571 (1997).
[17] H. L. Zhang, S. N. Nahar, and A. K. Pradhan (unpublished).
[18] H. L. Zhang and A. K. Pradhan, J. Phys. B **28**, 3403 (1995).
[19] H. L. Zhang and A. K. Pradhan, Astron. Astrophys. Suppl. Ser. **126**, 373 (1997).
[20] M. A. Bautista and A. K. Pradhan, Astron. Astrophys. Suppl. Ser. **126**, 365 (1997).
[21] W. Eissner, M. Jones, and N. Nussbaumer, Comput. Phys. Commun. **8**, 270 (1974).
[22] Yu Yan and M. J. Seaton, J. Phys. B **20**, 6409 (1987).
[23] M. A. Bautista, Astron. Astrophys., Suppl. Ser. **119**, 105 (1996).
[24] D. T. Woods, J. M. Shull, and C. L. Sarazin, Astrophys. J. **249**, 399 (1981).
[25] A. Burgess, Astrophys. J. **141**, 1588 (1965); **249**, 399 (1981).
[26] Y. Hahn, J. Quant. Spectrosc. Radiat. Transf. **41**, 315 (1989).
[27] V. L. Jacobs, J. Davis, P. C. Keppler, and M. Blaha, Astrophys. J. **215**, 690 (1977).
[28] M. J. Seaton, Yu Yan, D. Mihalas, and A. K. Pradhan, Mon. Not. R. Astron. Soc. **266**, 805 (1994).
[29] S. N. Nahar and A. K. Pradhan, Astrophys. J., Suppl. Ser. **111**, 339 (1997).
[30] S. N. Nahar, Astrophys. J. Suppl. (to be published).
[31] S. N. Nahar, Astrophys. J., Suppl. Ser. **106**, 213 (1996).
[32] All data may be obtained from the first author at nahar@astronomy.ohio-state.edu, and details of other related works may be obtained from the WWW site at http://www.astronomy.ohio-state.edu/~pradhan.